Epilepsy & Behavior 140 (2023) 109084

Contents lists available at ScienceDirect

Epilepsy & Behavior

journal homepage: www.elsevier.com/locate/yebeh

Midbrain structure volume, estimated myelin and functional connectivity in idiopathic generalised epilepsy

Andrea McKavanagh [a,b,*], Adam Ridzuan-Allen [a,b], Barbara A.K. Kreilkamp [a,b,c], Yachin Chen [h], José V. Manjón [d], Pierrick Coupé [e], Martyn Bracewell [b,f], Kumar Das [b], Peter N. Taylor [g], Anthony G. Marson [a,b], Simon S. Keller [a,b]

[a] Department of Pharmacology and Therapeutics, Institute of Systems, Molecular and Integrative Biology, University of Liverpool, Liverpool, UK
[b] The Walton Centre NHS Foundation Trust, Liverpool, UK
[c] Department of Neurology, University Medical Centre Göttingen, Göttingen, Germany
[d] Instituto de Aplicaciones de las Tecnologías de la Información y de las Comunicaciones Avanzadas (ITACA), Universitat Politècnica de València, Valencia, Spain
[e] Pictura Research Group, Unité Mixte de Recherche Centre National de la Recherche Scientifique (UMR 5800), Laboratoire Bordelais de Recherche en Informatique, Bordeaux, France
[f] Schools of Medical Sciences and Psychology, Bangor University, Bangor, UK
[g] Interdisciplinary Computing and Complex BioSystems Group, School of Computing Science, Newcastle University, UK
[h] Athinoula A. Martinos Center for Biomedical Imaging, Department of Radiology, Massachusetts General Hospital', United States

ARTICLE INFO

Article history:
Received 8 September 2022
Revised 1 January 2023
Accepted 1 January 2023

Keywords:
Midbrain
MRI
Substantia nigra
Subthalamic nucleus
Red nucleus

ABSTRACT

Background: Structural and functional neuroimaging studies often overlook lower basal ganglia structures located in and adjacent to the midbrain due to poor contrast on clinically acquired T1-weighted scans. Here, we acquired T1-weighted, T2-weighted, and resting-state fMRI scans to investigate differences in volume, estimated myelin content and functional connectivity of the substantia nigra (SN), subthalamic nuclei (SubTN) and red nuclei (RN) of the midbrain in IGE.

Methods: Thirty-three patients with IGE (23 refractory, 10 non-refractory) and 39 age and sex-matched healthy controls underwent MR imaging. Midbrain structures were automatically segmented from T2-weighted images and structural volumes were calculated. The estimated myelin content for each structure was determined using a T1-weighted/T2-weighted ratio method. Resting-state functional connectivity analysis of midbrain structures (seed-based) was performed using the CONN toolbox.

Results: An increased volume of the right RN was found in IGE and structural volumes of the right SubTN differed between patients with non-refractory and refractory IGE. However, no volume findings survived corrections for multiple comparisons. No myelin alterations of midbrain structures were found for any subject groups. We found functional connectivity alterations including significantly decreased connectivity between the left SN and the thalamus and significantly increased connectivity between the right SubTN and the superior frontal gyrus in IGE.

Conclusions: We report volumetric and functional connectivity alterations of the midbrain in patients with IGE. We postulate that potential increases in structural volumes are due to increased iron deposition that impacts T2-weighted contrast. These findings are consistent with previous studies demonstrating pathophysiological abnormalities of the lower basal ganglia in animal models of generalised epilepsy.

1. Introduction

Idiopathic generalised epilepsy (IGE) is a group of generalised epilepsy sub-syndromes that account for one-third of all epilepsies. The disorders are characterised by a presumed genetic predisposition, generalised spike/poly-spike wave discharges on EEG, and no identifiable brain lesion on routine MRI. IGEs are network disorders characterised by aberrant structural and functional brain networks which are thought to promote generalised ictal activity [1,2].

The basal ganglia (BG) are a cluster of interconnected subcortical nuclei that have been reported to play prominent roles in IGE ictal networks [3,4]. The BG act as critical hubs, receiving, relaying, and modulating information to and from the cortex via various neural pathways which include motor, sensory, dorsolateral prefrontal, lateral orbitofrontal, and anterior cingulate pathways [5].

* Corresponding author at: The BRAIN Lab, University of Liverpool Cancer Research Centre, 200 London Road, Liverpool L3 9TA, UK.
E-mail address: A.Mckavanagh@liverpool.ac.uk (A. McKavanagh).

https://doi.org/10.1016/j.yebeh.2023.109084
1525-5050/

Previous animal studies showed BG involvement in the propagation of epileptic discharges [6,7]. Furthermore, neuroimaging studies have reported morphometric [8,9], diffusion [9–11], and functional [3,4] MRI alterations of the BG in patients with IGE relative to healthy controls. Despite the clear involvement of BG nuclei in IGE, the focus of studies has almost entirely been on upper BG structures, such as the striatum and globus pallidus, to the exclusion of lower BG structures in the midbrain.

Lower BG structures include the substantia nigra (SN) and the subthalamic nucleus (SubTN). The primary reason that morphometric analyses of these structures in IGE are lacking is due to the poor contrast of these structures on clinically acquired isotropic T1-weighted images. The full anatomical profile of these structures, along with other midbrain structures such as the red nucleus (RN), are preferentially observed with isotropic T2-weighted images, which are not routinely acquired in patients with IGE. Despite this, there is convincing experimental evidence for the involvement of these structures in IGE.

Increased agonistic activation of nigral GABA receptors inhibits induced generalised motor seizure activity in male Sprague-Dawley rats [12]. Conversely, convulsive activity was not reduced when GABA receptor activation was increased in the striatum, hippocampus, or thalamus, suggesting that the SN is important for the inhibition of generalised seizures [12]. Other work reported that a reduction of inhibitory GABAergic neurons in BG structures including the SN pars reticula (SNr) is likely to contribute to increased seizure susceptibility of flurothyl-induced seizures in a genetic mouse model (*Brd +/-)* of JME [13], further highlighting how the SN may be implicated in genetic models of generalised epilepsy. Additional to modifications of the GABAergic system in the lower midbrain, alterations to the dopaminergic system have been reported in patients with IGE. Reduced dopamine transporter (DAT) binding in the midbrain and specifically in the SN was found in patients with JME using Positron Emission Tomography [14]. However, no changes were observed in striatal DAT binding [14]. Other computational work has reported that the SN and SubTN are part of an integrated network that modulates the EEG presentation of absence seizures [15]. Furthermore, despite few studies linking the RN with generalised epilepsy, some animal work has suggested that the RN may have a role in the expression of generalised seizures. For example, GTCSs were triggered in a convulsant mouse model by low threshold stimulation of the RN and high threshold stimulation of SN [16]. Other work suggested that the RN may have a role in seizure inhibition during induced tonic-clonic seizures [17]. There is therefore evidence to suggest that midbrain structures could play an important role in the pathophysiology of IGE.

In the present study, we prospectively acquired MRI data using a multi-sequence protocol that included 3D isotropic T1-weighted (T1W), T2-weighted (T2W), and resting-state functional MRI (rsfMRI). Data were acquired from patients with refractory (continued seizures despite anti-seizure medication) and non-refractory (seizure-free) IGE patients and healthy controls. We used these data to investigate whether patients with IGE showed evidence of altered volume, estimated myelin, and functional connectivity of SN, SubTN, and RN. Furthermore, we explored whether SN, SubTN, and RN alterations are potential markers of pharmacoresistance by comparing imaging data between patients with refractory and non-refractory IGE.

2. Methods

2.1. Participants

Thirty-three patients with IGE and thirty-nine age and sex-matched healthy controls with no history of neurological or psychiatric disease were recruited into this study. Demographic information can be found in Table 1 and more detailed clinical characteristics including specific subsyndromes and medications regimes can be found in Table 2. All patients were diagnosed with IGE by an experienced neurologist based on the ILAE classification criteria [18], including patient history, seizure semiology, and characteristic generalised spike/polyspike wave discharges on EEG. Ten patients were categorised as non-refractory, defined as being seizure free for 12 months at the time of recruitment [19]**.** Refractory patients experienced two or more seizures during the 12 months immediately prior to recruitment [19] and had failed more than two anti-seizure medication regimes. Participants were scanned at the Department of Neuroradiology at The Walton Centre NHS Foundation Trust and informed written consent was obtained for each (local research ethical committee reference 14/NW/0332).

2.2. Image acquisition

Each participant underwent an MRI protocol that consisted of T1W, T2W, and rsfMRI sequences using a 3T GE Discovery MR 750 MRI scanner with a 32-channel head coil: (1) T1W; fast spoiled gradient echo (FSPGR) images with Phased Array Uniformity Enhancement (PURE) signal inhomogeneity correction (140 slices, TR = 8.2 ms, TI = 450 ms, TE = 3.22 ms, flip angle = 12, with 1 mm isotropic voxel size, acquisition time: 3:48 mins); (2) T2W; T2W CUBE images (with PURE correction, 312 slices, TR = 2500 ms, TI = N/A, TE = 71.2 ms, flip angle = 90, with 0.5 mm isotropic voxel size); (3) rsfMRI; T2W Pulse sequence gradient echo, TE = 25 ms; TR = 2,000 ms; FOV = 24; slice thickness = 2. 4 mm; voxel size = 3.75 mm × 3.75 mm; 180 volumes; 38 slices; flip angle = 75, acquisition time: 6 mins. All participants were awake and instructed to look at a visual fixation point during scanning acquisition.

2.3. Segmentation and volumetry

Fig. 1 provides an overview of the image analysis pipeline used in the present study. Automatic segmentation software pBrain was used to automatically segment the SN, SubTN, and RN from T2W scans [20]. The software efficiently and accurately segments structures using multi-atlas label fusion technology on T2W scans as deep brain structures are more easily detectable on T2W scans than other imaging modalities [20]. Prior to segmentation, T2W images were rigidly aligned to T1W images using FSL FLIRT (FMRIB Software Library v6.0; https://fsl.fmrib.ox.ac.uk/fsl/fslwiki/FLIRT). Co-registered T2W images were then processed using pBrain and volumes of associated structures were calculated by the segmentation tool.

2.4. Constructing binary masks

Binary masks of segmentations were generated using FSL utilities to be used for further downstream myelin and connectivity analysis (Fig. 1.B). Structures were assigned a numerical label from the segmentation software which was used as an absolute threshold to remove voxels with intensity values above/below the thresholded value. Subsequently, thresholded segments were binarized using FSL utilities by retaining non-zero voxels only, generating binary masks for all structures. All binary masks were checked manually for segmentation accuracy.

2.5. Estimated myelin content

Myelin content was estimated using a whole-brain myelin mapping technique [21]. MRI contrast in cortical grey matter is

Table 1
Participant demographic and clinical characteristics.

	Groups				Stats	
	Healthy Controls	*All Patients*	*Ref*	*Non-Ref*	HC vs All	Ref vs Non-Ref
N	39	33	23	10	-	-
Sex F/M (n,%)	23(59)/16(41)	18(55)/15(45)	13(56)/10(44)	5(50)/5(50)	0.81	>0.99
Mean age (±SD)	32(8.6)	32(15)	35(15)	26(11)	0.13	0.08
Mean age at Onset (±SD)	-	13(5.6)	14(5.4)	12(5.9)	-	0.61
Mean epilepsy Duration (±SD)	-	19(16)	21(16)	14(16)	-	0.10

Sex significance calculated using Fisher's Exact test and Age/Onset/Duration significance using Mann Whitney U test; Ref = Refractory; Non-ref = Non-refractory; Age/Onset and Duration in years; significance = $p < 0.05$.

Table 2
Detailed clinical characteristics of patients.

Patient	Age	Sex	Onset	Duration	Category	FH	PS	Seizures	ASM(mg/day)
1	23	F	14	9	Ref	N	N	AS, MS	LEV 300, TOP 300, Clob 10
2	19	M	16	3	Ref	Y	Y	GTCS	VPA 1000
3	19	F	8	11	Ref	Y	N	AS, GTCS	LTG 200
4	25	M	19	6	Non-Ref	N	N	MS	LEV1500, VPA 1600
5	60	F	13	47	Ref	Y	N	AS, GTCS	VPA 2500
6	24	M	15	9	Ref	Y	N	AS, MS, GTCS	CBZ1000, LEV 3000, VPA 2500
7	21	F	15	6	Ref	N	N	AS, MS, GTCS	LEV 4000, VPA 2000
8	32	F	23	9	Ref	Y	N	MS, GTCS	LEV 3500, Clob 15
9	38	M	18	20	Ref	Y	N	GTCS	VPA 600, LTG 50
10	67	M	29	38	Ref	N	N	AS, GTCS	VPA 2000, LTG 200, PB 150, Clob 10
11	46	F	7	39	Ref	N	N	AS	VPA 1200, LTG 200, LEV 2500
12	20	M	8	12	Ref	N	N	GTCS	VPA 2000
13	24	F	13	11	Ref	Y	N	MS, GTCS	TOP 100
14	35	M	6	29	Ref	N	N	GTCS	LEV 2000, VPA 2000
15	18	M	14	4	Ref	N	N	AS, GTCS	VPA 1500, ZON 350
16	39	M	17	22	Ref	Y	Y	GTCS	VPA 1000, LTG 75
17	24	F	16	8	Non-Ref	N	N	AS, GTCS	VPA 1000, LTG 200, LEV 4000
18	21	M	16	5	Ref	N	N	AS, MS, GTCS	VPA 2400
19	36	F	17	19	Ref	N	N	GTCS	LEV 1250, TOP 100
20	31	F	16	16	Ref	N	N	GTCS	LEV 2000, LTG 400
21	31	F	17	15	Ref	N	N	AS, MS, GTCS	VPA 1500, LEV 3500
22	23	M	16	7	Non-Ref	N	N	AS, GTCS	VPA 2100, LEV 500
23	19	F	13	6	Non-Ref	Y	N	GTCS	LEV 3000
24	58	F	15	43	Ref	N	N	GTCS	VPA 1000, ZON 400, Clon 1.5
25	18	F	15	3	Non-Ref	N	Y	AS, MS	LEV 2000
26	22	M	2	20	Non-Ref	N	Y	AS, MS	VPA 1400
27	24	M	13	11	Ref	N	N	MS	VPA 1700
28	56	F	3	53	Non-Ref	N	Y	AS	VPA 1500
29	57	F	7	50	Ref	N	N	AS, GTCS	VPA 1200, CBZ 600
30	33	M	7	26	Non-Ref	N	N	AS	VPA 1800
31	19	F	14	5	Non-Ref	N	N	AS, MS	LEV 1000
32	57	F	7	50	Ref	Y	N	GTCS	VPA 2000, LTG 75
33	20	M	16	4	Non-Ref	N	N	AS, GTCS, MS	VPA 1700, ETX 500

Onset = age at onset of epilepsy in years; Duration = Duration of epilepsy in years; F = female; M = male; Ref = refractory; Non-Ref = Non-Refractory; FH = family history; PS = photosensitive; ASM = anti-seizure medication; AS = absence seizures; GTCS = primary generalized tonic-clonic seizures; MS = myoclonic seizures; VPA = Valproic acid; ZON = Zonisamide; LEV = Levetiracetam; TOP = Topiramate; Clob = Clobazam; Clon = Clonazepam; LTG = Lamotrigine; CBZ = Carbamazepine; PB = Phenobarbital; ETX = Ethosuximide; N = no; Y = yes.

influenced by iron depositions, and myelin content and iron are colocalised [22]. It has therefore been suggested that grey matter myelin content can be indirectly measured using MRI signal intensities [21]. Grey matter myelin inversely covaries with T1W and T2W signal intensity, while background noise does not correlate between the two modalities. Thus, Glasser and colleagues proposed a straightforward non-invasive methodology for measuring estimated myelin content using a ratio of T1W/T2W image intensities (Equation 1), while removing the need for bias field correction due to inhomogeneous MRI signals, and enhancing the contrast to noise ratio for myelin content [21]:

$$\frac{T1W}{T2W} \approx \frac{x * b}{(1/x) * b} = x^2$$

Equation 1. Where x = myelin content in T1W image, 1/x = myelin content in T2W image (inverse of T1W), b = receive bias field in both images, and x^2 = enhanced myelin contrast image (T1W/T2W image).

Image pre-processing and whole-brain myelin mapping were carried out according to the previously described method [21]. Subsequently, lower basal ganglia and midbrain binary masks were applied to the myelin-enhanced T1W/T2W images (Fig. 1. C), and the median voxel signal values within each mask were calculated using FSL utilities to determine the myelin content per segmented structure.

2.6. Statistical analysis of volumetry and myelin estimation

Permutation testing via FSL toolbox PALM (https://fsl.fmrib.ox.ac.uk/fsl/fslwiki/PALM) was used to compare midbrain volume/myelin content between groups. The software constructs a standard linear model for the observed parameters and calculates a t-statistic for each contrast (IGE vs controls; non-refractory vs refrac-

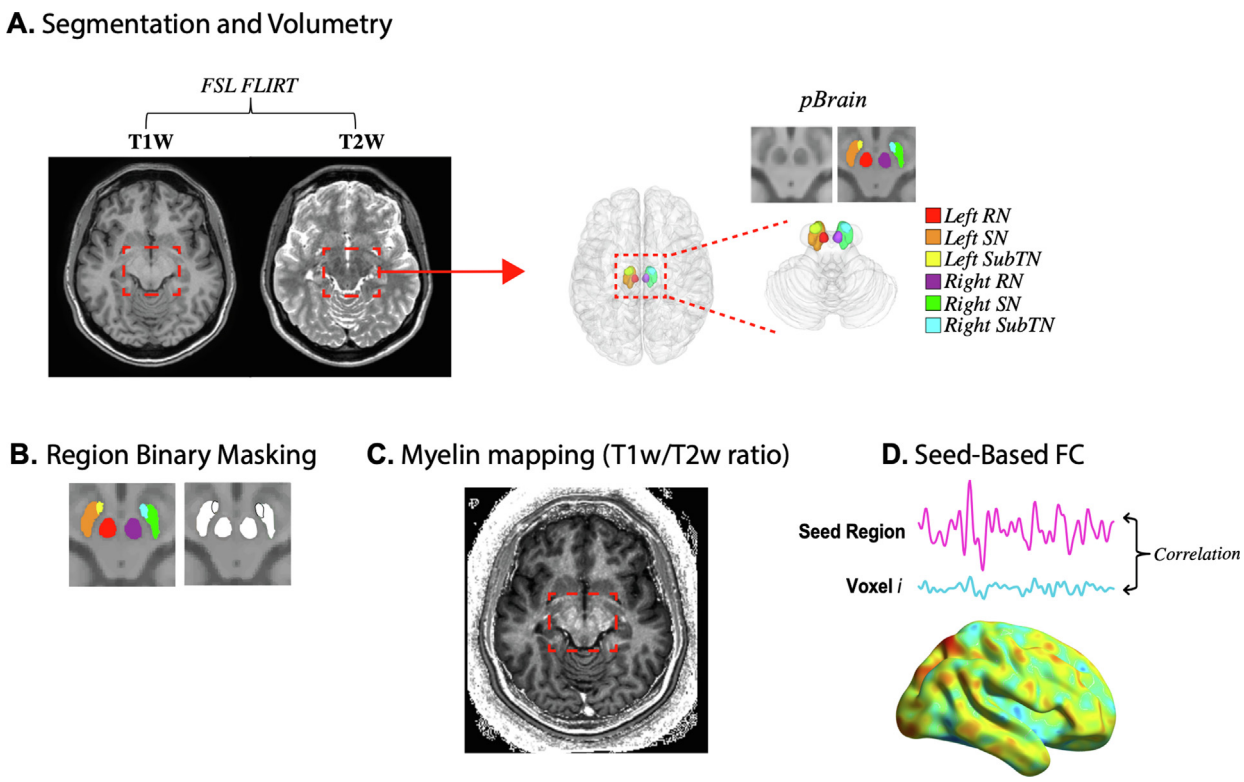

Fig. 1. Methods pipeline schematic. (A) T2W images are rigidly aligned to T1W images prior to input into automatic segmentation software pBrain, which segments and computes midbrain structure volumes. (B) Segmented regions are thresholded, binarized, and masked. (C) Myelin estimation maps are generated from a T1W/T2W ratio computation. Regional masks are overlayed onto myelin maps to extract overall myelin content per region per subject using FSL utilities. (D) Structural masks are used as seeds in rsfMRI seed-based functional connectivity analysis.

tory), then the model is permuted (10,000 iterations) and a p-value computed (FDR corrected). All parameters were corrected for age and sex using a GLM prior to permutation testing, and volumes were also corrected for ICV (as calculated by pBrain).

2.7. Resting-State fMRI pre-processing

rsfMRI data were pre-processed using Statistical Parametric Mapping software (SPM12, Welcome Trust Centre for Neuroimaging, London, UK; https://www.fil.ion.ucl.ac.uk/spm/). Pre-processing steps included slice time correction of the 180 volumes using the first volume as a reference. Head motion and EPI distortion were corrected using the spatial realignment and unwarp tools, respectively. A motion artifact threshold (translation > 3 mm, rotation > 1°) was applied which caused the exclusion of five controls due to excessive head motion. Subsequently, scans were spatially normalised to the ICBM 152 template using an affine registration and then smoothed with an 8 mm full width at half maxima (FWHM) gaussian kernel to increase the signal-to-noise ratio. T1W images were skull stripped and segmented into grey matter, white matter, and cerebrospinal fluid (CSF) using the SPM Computational Anatomy Toolbox (CAT12; https://www.neuro.uni-jena.de/cat/), and all segmentations were non-linearly registered to the ICBM 152 template. Pre-processing was completed using the SPM Functional Connectivity Toolbox (CONN; https://web.conn-toolbox.org, integrated in SPM12. As part of CONN's default denoising pipeline to prevent potential confounding effects, nuisance variables including the first 5 principal components of white matter and CSF signals, and 6 motion parameters including their associated first-order derivates, were linearly regressed out using Ordinary Least Squares (OLS) regression. Furthermore, a band-pass filter (0.01–0.08 Hz) was applied to control for scanner drift and high-frequency physiological noise.

2.8. Seed-based functional connectivity and statistical analysis

Seed-based connectivity (SBC) maps for each participant were computed between midbrain seeds and all other grey matter voxels. First, masks were linearly transformed to MNI space using SPM normalise and registration accuracy was checked manually. Standard space masks were then imported into the CONN toolbox and used as seeds of interest in the rsfMRI seed-based functional connectivity. A Fisher-transformed correlation coefficient between the average BOLD signal of the seed and the BOLD signal of every grey matter voxel within the rest of the brain was calculated. Cluster-level statistics using Random Field Theory were applied in CONN to the SBC maps of each midbrain region to compare results between subject groups (IGE vs controls; non-refractory vs refractory). A statistical parametric map (corrected for age and sex) of t-values estimated using a GLM was generated and thresholded to $p < 0.001$ to define clusters. The size of each cluster (number of voxels) was measured and compared to a known probability density function to give each cluster a p-value which underwent multiple comparison correction using the false discovery rate (FDR). The significance for clusters was thresholded at $p < 0.05$ (FDR-corrected).

3. Results

3.1. Red nucleus

An increased volume of the right RN ($t = 2.11$, $p = 0.03$) was found in patients with IGE compared to controls (Fig. 2.A; Table 3), although this finding did not survive multiple comparison correction (pFDR = 0.15). No volume alterations of the RN were found between patients with refractory and non-refractory IGE and no

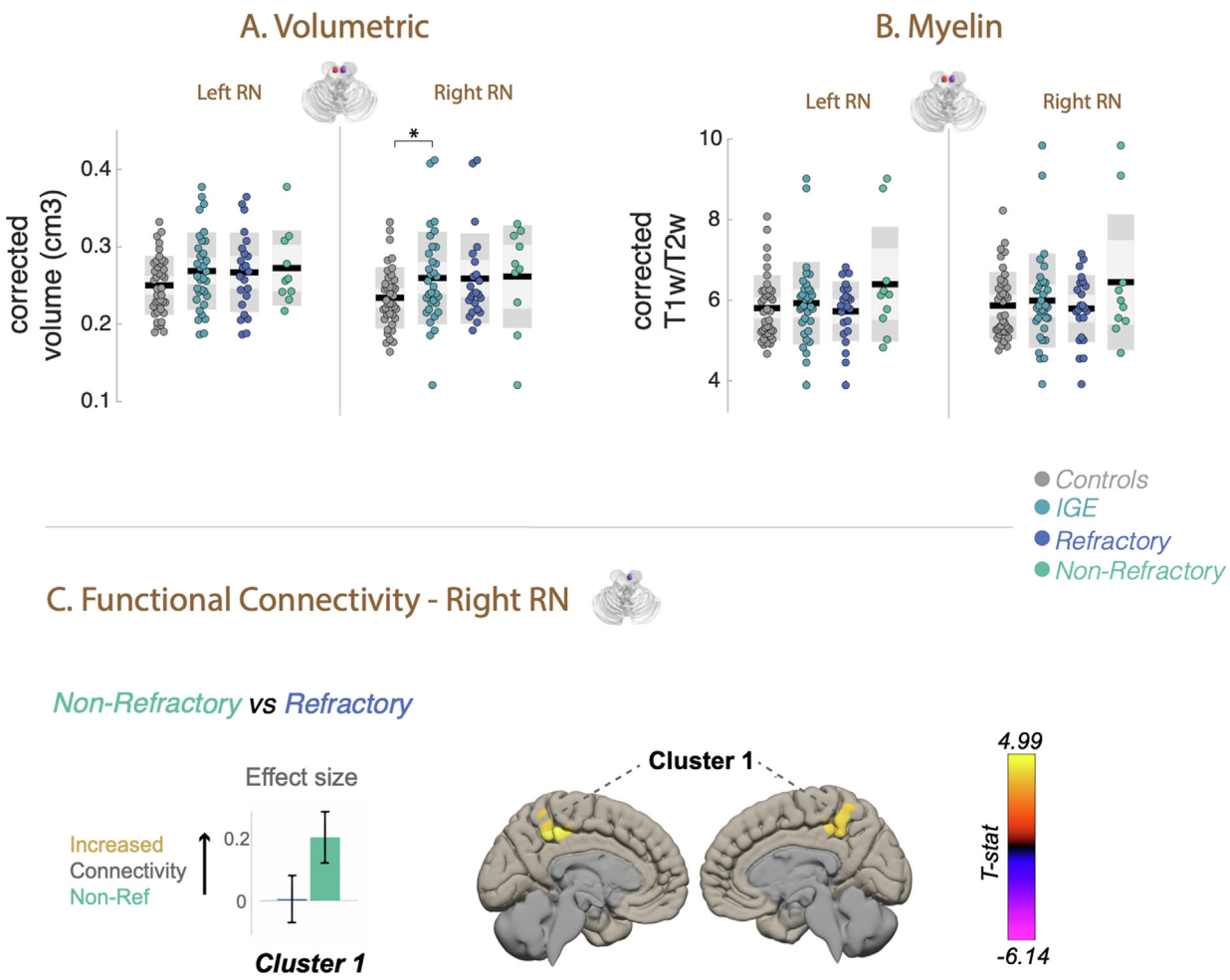

Fig. 2. Volume, myelin estimation, and functional connectivity of the red nucleus (RN) bilaterally in patients with IGE. (A) Volumes (cm^3) of the left and right RN for subject groups. All volumes were corrected for age, sex and ICV. (B) Myelin estimation (ratio T1W/T2W) of the left and right RN for subject groups. Estimated myelin was corrected for age and sex. (C) Functional connectivity differences (pFDR < 0.05, cluster corrected) of the right RN between patients with non-refractory and refractory IGE. Bar charts show effect size differences, 90% confidence intervals, and direction of contrast for subject group pairs. Cluster colour indicates the t-score and trend direction (increased/decreased connectivity). (RN = red nucleus; * = p < 0.05).

significant myelin alterations were found between subject groups (Fig. 2.B; Table 4). Significantly increased functional connectivity was observed between the right RN and the left and right precuneus cortex in patients with refractory IGE relative to those with non-refractory IGE (Fig. 2.C; Table 5).

3.2. Subthalamic nucleus

Patients with non-refractory IGE had a decreased volume of the right SubTN (t = −2.12, p = 0.04) relative to patients with non-refractory IGE (Fig. 3.A; Table 3), although this finding did not survive multiple comparison correction (pFDR = 0.23). No significant volume differences were found between patients and controls, and no myelin alterations were found between subject groups (Fig. 3.B; Table 4). Significantly increased functional connectivity was observed between the right SubTN and the left superior frontal gyrus in patients with IGE relative to controls (Fig. 3.C; Table 5). Additionally, patients with non-refractory IGE had significantly decreased connectivity between the left SubTN and right lateral occipital cortex compared to patients with refractory IGE.

3.3. Substantia nigra

No significant volume or myelin alterations of the SN were found between patients with IGE and controls or between patients with refractory and non-refractory IGE (Fig. 4.A and B; Table 3; Table 4). Patients with IGE had significantly decreased functional connectivity between the left SN and the bilateral thalamus and caudate nucleus compared to controls (Fig. 4.C; Table 5). Compared to patients with refractory IGE, patients with non-refractory IGE had significantly increased connectivity between the left SN and the left cerebellum and decreased connectivity between the left SN and the right cerebellum.

4. Discussion

We investigated whether volume, estimated myelin, and functional connectivity of the lower BG structures located within and adjacent to the midbrain is altered in patients with IGE. We found patients with IGE had increased volumes of the RN and SubTN, although these effects did not survive multiple comparison correction. We observed functional connectivity alterations of the SN, SubTN, and RN in patients with IGE compared to healthy controls. Furthermore, we observed volumetric alterations and differential patterns of functional connectivity between patients with non-refractory and refractory IGE.

Previous studies reported MRI-determined volumetric changes of upper BG structures including the striatum and pallidum in patients with IGE [8,9]. To our knowledge, we are the first to inves-

Table 3
Comparison of volumes between subject group pairs using FSL PALM.

	All Patients (N = 33)		Refractory (N = 23)		Non-Refractory (N = 10)		Healthy Controls (N = 39)		All Patients vs Controls			Non-Refractory vs Refractory		
Region	*Mean volume (cm3)*	*SD*	*Mean volume (cm3)*	*SD*	*Mean volume (cm3)*	*SD*	*Mean volume (cm3)*	*SD*	*tval*	*pval*	*pFDR*	*tval*	*pval*	*pFDR*
Left RN	0.26	0.06	0.25	0.06	0.29	0.06	0.24	0.04	1.80	0.07	0.15	0.34	0.73	0.99
Right RN	0.25	0.07	0.25	0.07	0.27	0.07	0.23	0.04	2.11	*0.03	0.15	0.14	0.89	0.99
Left SubTN	0.11	0.07	0.11	0.08	0.12	0.02	0.09	0.02	1.00	0.36	0.43	−0.90	0.32	0.96
Right SubTN	0.11	0.03	0.11	0.04	0.11	0.02	0.10	0.02	−0.06	0.95	0.95	−2.12	*0.04	0.23
Left SN	0.54	0.15	0.53	0.17	0.54	0.10	0.50	0.08	1.09	0.28	0.42	−0.32	0.75	0.99
Right SN	0.49	0.11	0.48	0.12	0.51	0.10	0.44	0.08	1.88	0.06	0.15	0.02	0.99	0.99

RN = Red Nucleus; SubTN = Subthalamic Nucleus; SN = Substantia Nigra; SD = standard deviation; FDR = False discovery rate; Significance = $p < 0.05$; * = uncorrected significance.

Table 4
Comparisons of myelin content between subject group pairs using FSL PALM.

	All Patients (N = 33)		Refractory (N = 23)		Non-Refractory (N = 10)		Healthy Controls (N = 39)		All Patients vs Controls			Non-Refractory vs Refractory		
Region	*Mean T1W/T2W*	*SD*	*Mean T1W/T2W*	*SD*	*Mean T1W/T2W*	*SD*	*Mean T1W/T2W*	*SD*	*tval*	*pval*	*pFDR*	*tval*	*pval*	*pFDR*
Left RN	5.91	1.00	5.77	0.70	6.23	1.48	5.79	0.84	1.15	0.26	0.33	1.99	0.05	0.23
Right RN	5.98	1.14	5.84	0.78	6.28	1.74	5.85	0.84	1.04	0.31	0.33	1.76	0.08	0.23
Left SubTN	6.69	1.18	6.63	0.92	6.84	1.68	6.53	0.94	0.99	0.33	0.33	1.13	0.26	0.31
Right SubTN	6.76	1.28	6.69	0.95	6.93	1.89	6.48	0.98	1.39	0.17	0.33	1.13	0.26	0.31
Left SN	5.93	1.16	5.90	0.96	6.01	1.60	5.70	0.90	1.22	0.23	0.33	0.91	0.36	0.36
Right SN	5.81	1.15	5.73	0.88	5.99	1.67	5.64	0.92	1.04	0.30	0.33	1.24	0.22	0.31

RN = Red Nucleus; SubTN = Subthalamic Nucleus; SN = Substantia Nigra; SD = standard deviation; FDR = False discovery rate; Significance = $p < 0.0$; * = uncorrected significance.

Table 5
Midbrain Functional Connectivity Results.

Seed Region	Subject Groups	Cluster Number	Connectivity Direction	Cluster Brain Region	x	y	z	Voxels	pFDR
Right RN	Non-Refractory vs Refractory	Cluster 1	+	Precuneus Cortex	−2	−40	46	227	0.00
Left SubTN	Non-Refractory vs Refractory	Cluster 1	-	Right Lateral Occipital Cortex	38	−82	34	206	0.00
Right SubTN	All Patients vs Controls	Cluster 1	+	Left Superior Frontal Gyrus Left Precentral Gyrus	−14	−6	74	143	0.02
Left SN	All Patients vs Controls	Cluster 1	-	Right Thalamus Right Caudate	16	−20	16	114	0.04
		Cluster 2	-	Left Thalamus Left Caudate	−8	−4	16	113	0.04
	Non-Refractory vs Refractory	Cluster 1	+	Left Cerebellum	−12	−66	−46	120	0.01
		Cluster 2	-	Right Cerebellum	10	−34	−14	108	0.01

Red Nucleus; SubTN = Subthalamic Nucleus; SN = Substantia Nigra; -/+ = decreased/increased connectivity.

tigate the structure of the SN, SubTN, and RN in patients with IGE using MRI. We found uncorrected volumetric increases of the right RN and the right SubTN. Both the RN and SubTN are known to modulate motor movement and play a role in motor disorders [23,24], and therefore have the potential to play an important motoric role in the initiation and termination of seizures in epilepsy. Increased regional volumes on T1W images have been commonly found previously in IGE, including in the thalamic nuclei (*c.f.* more studies report thalamic volume reduction rather than volume increase, Chen et al., 2021), the right medial frontal gyrus, right anterior cingulate cortex [25], precentral gyrus and paracentral lobule [26]. The underlying causes of increased structural volume in IGE are not clear. It has been hypothesised that T1W-derived grey matter increases may have been caused by consequences of functional alterations, or by histopathological alterations such as microdygenesis [27]. Despite those hypotheses, there have been no MRI volumetric studies on the SN, SubTN, and RN in patients with IGE. Volumetric increases of the RN have been reported previously in Parkinson's disease and authors have hypothesised volume alterations may be related to an increase in iron content in the region [28]. In terms of epilepsy, a review of the literature reported correlations between epilepsy and iron metabolism [29]. An accumulation of iron, altered iron metabolism, and iron-induced inflammation has been reported in post-mortem brain tissue of patients with TLE [30]. In addition to increased volumetric findings in this study, results are lateralised to the right hemisphere. Previous studies in IGE have found lateralized grey and white matter alterations, including decreased thalamic volumes specific to the right side [31], reduced hippocampal volumes more extensive on the left side [32], and asymmetry of FA alterations [33]. Despite the bilateral nature of IGE, the disorder can present with lateralised motor manifestations [34], asymmetric seizure termination [35], and cortical focal onsets of GSWD [36–39] which suggests generalised epilepsy may affect hemispheres differently. Overall, the exact pathophysiological correlates of volumetric increases and potential lateralisation mechanisms in IGE remain unknown, therefore further research of the structures of the lower BG and midbrain nuclei, with the use of high-resolution T2W images, is warranted.

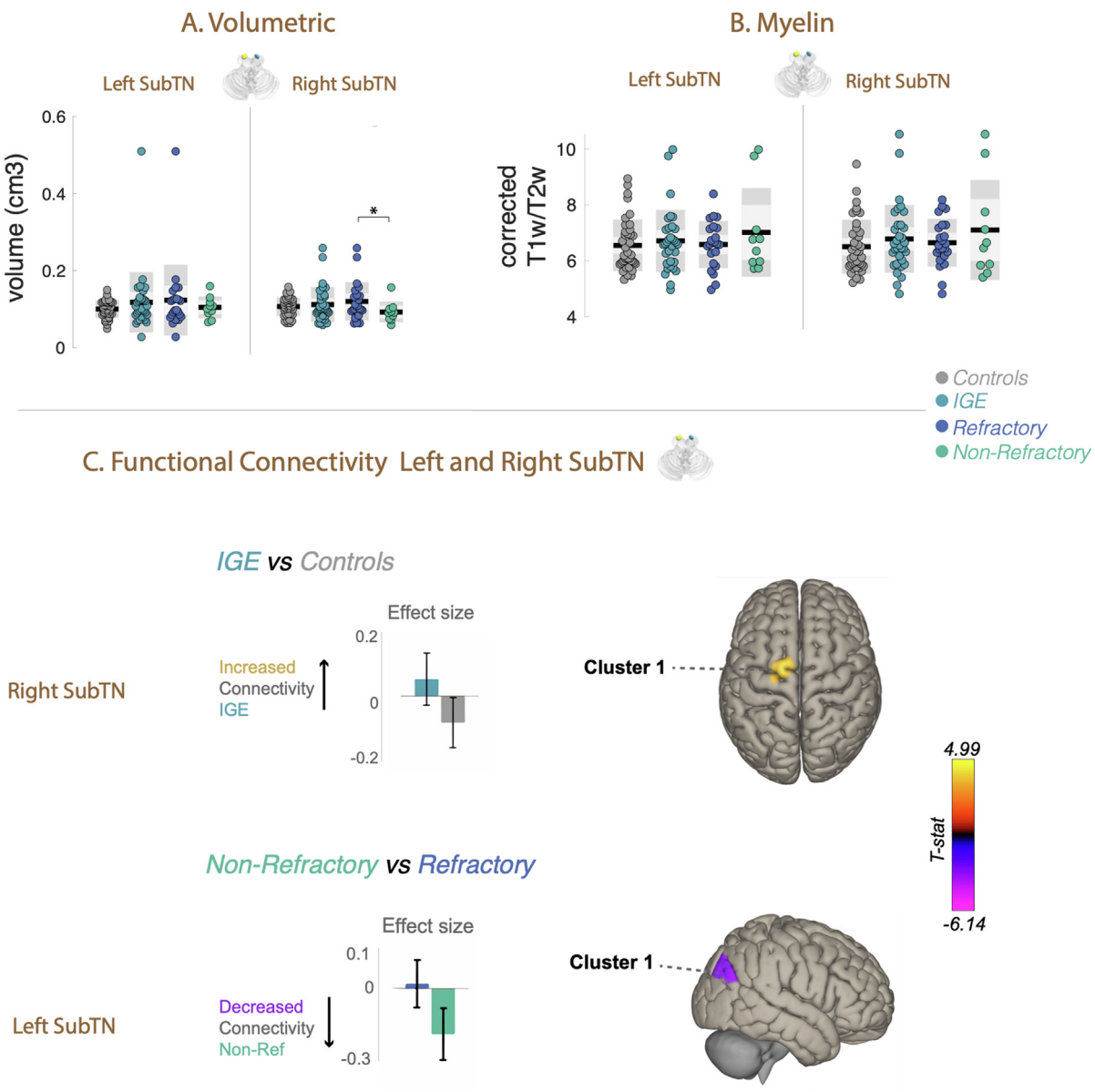

Fig. 3. Volume, myelin estimation, and functional connectivity of the subthalamic nucleus (SubTN) bilaterally in patients with IGE. (A) Volumes (cm^3) of the left and right SubTN for subject groups. All volumes were corrected for age, sex and ICV. (B) Myelin estimation (ratio T1W/T2W) of the left and right SubTN for subject groups. Estimated myelin was corrected for age and sex. (C) Functional connectivity differences (pFDR < 0.05, cluster corrected) of the right SubTN of patients with IGE relative to controls, and the left SubTN between patients with non-refractory and refractory IGE. Bar charts show effect size differences, 90% confidence intervals, and direction of contrast for subject group pairs. Cluster colour indicates the t-score and trend direction (increased/decreased connectivity). (SubTN = Subthalamic Nucleus).

We found no evidence of changes to estimated myelin within midbrain nuclei in patients with IGE. Previous studies reported reduced estimated myelin in patients with epilepsy including right hemisphere epilepsy [40] and refractory epilepsy [41], and decreased myelin water fraction has been found in the frontal lobe white matter in patients with CAE [42]. Furthermore, those with disorders of myelin content have been found to have an increased susceptibility to having epileptic seizures [43,44]. Most studies focused on white matter tracts given the extensive axonal myelination in this area of the brain. Diffusion tensor imaging (DTI) studies have frequently been performed in patients with IGE and suggested a potential relationship between altered diffusion properties of white matter tracts and abnormal white matter myelination [10,11]. There is evidence to suggest that diffusion scalar metrics are sensitive to myelin content [45,46]. In contrast to previous white matter DTI studies, we analysed estimated myelin within midbrain grey matter nuclei, which has not been previously performed in patients with IGE. We used a well-established T1W/T2W ratio method which is sensitive to grey matter myelin content [21]. The absence of estimated myelin content differences in the SN, SubTN, and RN may be explained by different myelination patterns and myelination functions between white and grey matter [47]. It has been hypothesised grey matter myelinated axons may be used for metabolic reasons or as inhibitors of axonal sprouting rather than saltatory conduction as seen in the white matter [47]. Alternatively, it is also possible myelin is not impacted in the grey matter nuclei of the midbrain and lower BG in IGE.

We report subtle structural changes and no microstructural changes in IGE yet find significant functional connectivity alterations. Despite previous studies also finding structural changes in IGE with results often inconsistent between studies [25], global widespread network changes are commonly found in both struc-

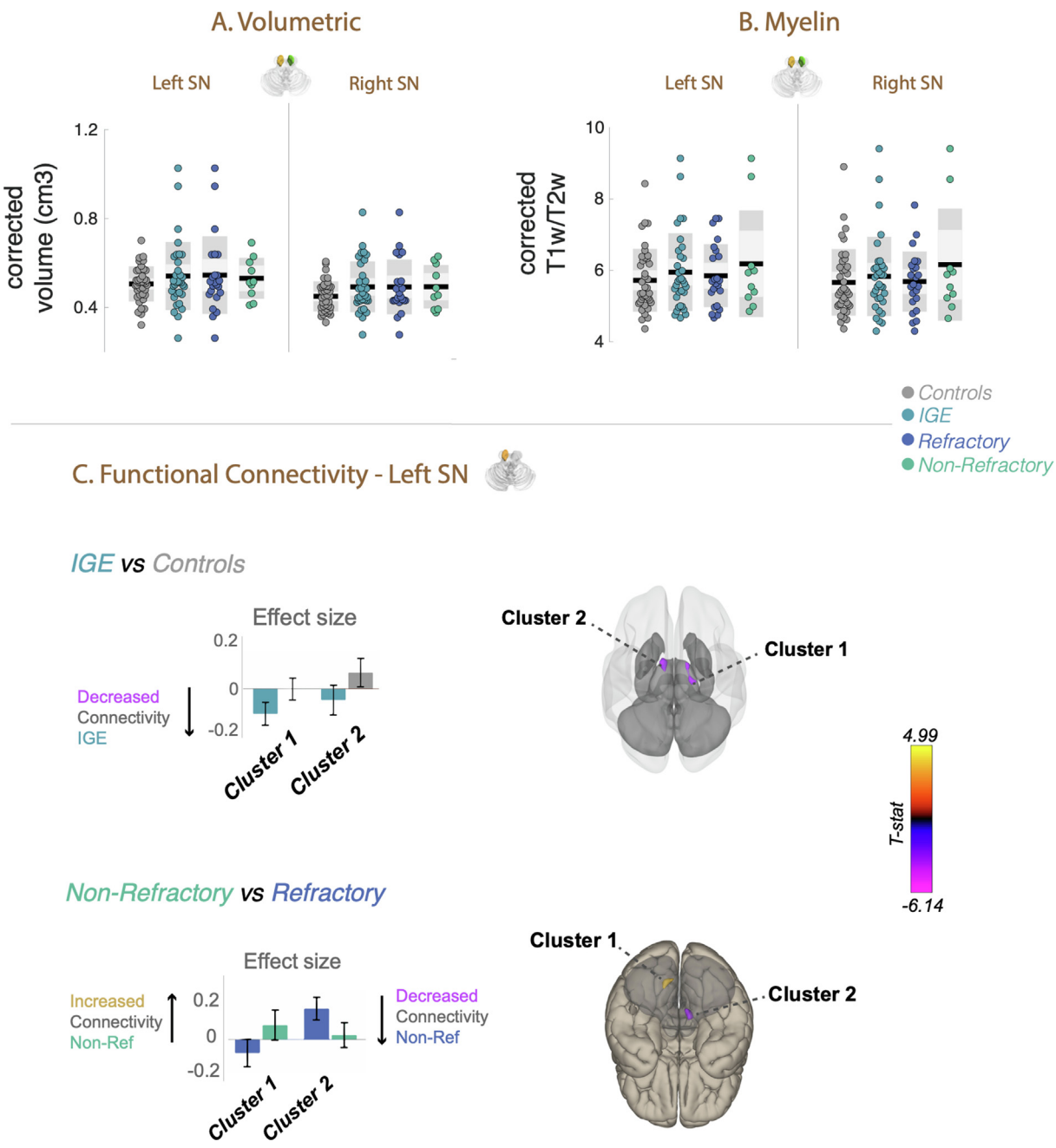

Fig. 4. Volume, myelin estimation, and functional connectivity of the substantia nigra (SN) bilaterally in patients with IGE. (A) Volumes (cm^3) of the left and right SN for subject groups. All volumes were corrected for age, sex and ICV. (B) Myelin estimation (ratio T1W/T2W) of the left and right SN for subject groups. Estimated myelin was corrected for age and sex. (C) Functional connectivity differences (pFDR < 0.05, cluster corrected) of the right SN between patients with non-refractory and refractory IGE. Bar charts show effect size differences, 90% confidence intervals, and direction of contrast for subject group pairs. Cluster colour indicates t-score and trend direction (increased/decreased connectivity). (SN = substantia nigra, * = p < 0.05).

tural and functional networks [48–50]. It has been suggested that global and local network alterations to the pre-seizure network facilitate seizure generation and has an effect on all network components including specific structures [51]. Therefore, all network components may be affected in IGE although it is possible local structural changes are more elusive and that network-level metrics are more sensitive to IGE pathophysiology.

We report decreases in functional connectivity between the SN and the thalamus and caudate in patients with IGE. However, diverging results have shown the SN, thalamus, and caudate are more intrinsically functionally connected as part of the BG resting state network in patients with IGE compared to controls [4]. Alternative results may be explained by different methodological approaches used between studies (spatial ICA vs localised seed-based temporal correlation analysis used here). Functional alterations found between the midbrain, thalamus, and caudate are unsurprising as the SN modulates the direct and indirect pathway to initiate/inhibit motor movement looping signals to the cortex via interactions with the BG [5]. Decreased functional connectivity of the SN highlights the weaker integration of these nuclei within motor pathways, which may be a factor in the clinical manifestations of seizures in IGE.

We found increased functional connectivity between the right SubTN and the left superior frontal gyrus in patients with IGE.

Probabilistic tractography has established projection fibers exist between both structures as part of the hyper direct pathway for the modulation of motor movement [52]. The importance of these interconnected white matter tracts for movement has been evidenced by their role in the deep brain stimulation of the SubTN in Parkinson's disease [53]. The superior frontal gyrus has been found to be impaired in patients with IGE, with previously reported microstructural alterations [54] and epileptiform discharges [55]. Therefore, abnormal connectivity between the SubTN and superior frontal gyrus may be related to altered networks contributing to the motor manifestations of seizures in IGE.

We also found connectivity alterations characteristic of patients with non-refractory IGE. We observed decreased connectivity between the left SubTN and the right lateral occipital cortex and increased functional connectivity between the right RN and precuneus compared to patients with refractory IGE. Cognitive dysfunction, ongoing cognitive decline, and more severe cognitive impairment are found in patients with refractory epilepsy [56]. Functional circuits for visuospatial processing involve both the SubTN and occipital lobe in humans [57]. The RN is similarly involved in cognitive circuits including episodic memory function and is functionally connected to the precuneus cortex [58]. Furthermore, we observed connectivity alterations between the SN and cerebellum in patients with non-refractory IGE. Connectivity alterations between the cerebellum and BG structures have been found previously in IGE [59] and the cerebellum has been reported to be a modulator of generalised seizures [60]. These network connectivity alterations may be implicated in cognitive impairments and motor control in IGE and thus in non-refractory patients may suggest possible changes in cognitive and motor circuits indicative of seizure freedom.

5. Limitations

There are several limitations of this study. Different medication regimes between patients may influence results as some antiepileptic drugs can decrease cerebral blood flow [61] which may impact BOLD signal and functional connectivity. However, this effect may be specific to certain resting-state networks as limited antiepileptic drug effects on functional connectivity of the BG network have been found previously in IGE [4]. Furthermore, our patient sample includes several sub-disorders of IGE which may influence results due to possible syndrome-specific pathophysiological mechanisms. However, shared similarities between IGE sub-syndromes including, clinical features [62] and some pathophysiological mechanisms [63] have previously been found. Therefore, investigating volumetric, myelin, and functional similarities between sub-syndromes is important. Lastly, low spatial resolution of fMRI and the small size of midbrain nuclei investigated may decrease the reliability of the BOLD signal in the midbrain area, therefore studies with an increased spatial resolution could account for this limitation in the future.

6. Conclusion

We report structural and functional connectivity alterations of midbrain structures in patients with IGE. Future studies are needed to confirm structural changes in the midbrain and their potential link to an increased iron accumulation in the region. Structural changes may relate to functional connectivity alterations that we observed between lower BG/midbrain structures and other cortical and subcortical grey matter areas.

Data availability

Data available on request from the authors.

Data availability

Data available on request from the authors.

Declaration of Competing Interest

The authors declare that they have no known competing financial interests or personal relationships that could have appeared to influence the work reported in this paper.

Funding and Acknowledgments

This work was supported by a UK Medical Research Council DiMeN DTP studentship awarded to AM. SSK acknowledges support from the UK Medical Research Council (Grant Number MR/S00355X/1).

References

[1] Larivière S, Rodríguez-Cruces R, Royer J, Caligiuri ME, Gambardella A, Concha L, et al. Network-based atrophy modeling in the common epilepsies: A worldwide ENIGMA study. Sci Adv 2020. https://doi.org/10.1126/sciadv.abc6457.
[2] Liu F, Wang Y, Li M, Wang W, Li R, Zhang Z, et al. Dynamic functional network connectivity in idiopathic generalized epilepsy with generalized tonic–clonic seizure. Hum Brain Mapp 2017;38(2):957–73. https://doi.org/10.1002/hbm.23430.
[3] Gong J, Jiang S, Li Z, Pei H, Li Q, Yao D, et al. Distinct effects of the basal ganglia and cerebellum on the thalamocortical pathway in idiopathic generalized epilepsy. Hum Brain Mapp 2021. https://doi.org/10.1002/hbm.25444.
[4] Luo C, Li Q, Xia Y, Lei X, Xue K, Yao Z, et al. Resting state basal ganglia network in idiopathic generalized epilepsy. Hum Brain Mapp 2012. https://doi.org/10.1002/hbm.21286.
[5] Simonyan K. Recent advances in understanding the role of the basal ganglia. F1000Research 2019. https://doi.org/10.12688/f1000research.16524.1.
[6] Deransart C, Riban V, Lê BT, Marescaux C, Depaulis A. Dopamine in the striatum modulates seizures in a genetic model of absence epilepsy in the rat. Neuroscience 2000. https://doi.org/10.1016/S0306-4522(00)00266-9.
[7] Slaght SJ, Paz T, Chavez M, Deniau JM, Mahon S, Charpier S. On the activity of the corticostriatal networks during spike-and-wave discharges in a genetic model of absence epilepsy. J Neurosci 2004. https://doi.org/10.1523/JNEUROSCI.1449-04.2004.
[8] Du H, Zhang Y, Xie B, Wu N, Wu G, Wang J, et al. Regional atrophy of the basal ganglia and thalamus in idiopathic generalized epilepsy. J Magn Reson Imaging 2011. https://doi.org/10.1002/jmri.22416.
[9] Keller SS, Ahrens T, Mohammadi S, Möddel G, Kugel H, Ringelstein EB, et al. Microstructural and volumetric abnormalities of the putamen in juvenile myoclonic epilepsy. Epilepsia 2011. https://doi.org/10.1111/j.1528-1167.2011.03117.x.
[10] Yang T, Guo Z, Luo C, Li Q, Yan B, Liu L, et al. White matter impairment in the basal ganglia-thalamocortical circuit of drug-naïve childhood absence epilepsy. Epilepsy Res 2012. https://doi.org/10.1016/j.eplepsyres.2011.12.006.
[11] Luo C, Xia Y, Li Q, Xue K, Lai Y, Gong Q, et al. Diffusion and volumetry abnormalities in subcortical nuclei of patients with absence seizures. Epilepsia 2011;52(6):1092–9. https://doi.org/10.1111/j.1528-1167.2011.03045.x.
[12] Iadarola MJ, Gale K. Substantia nigra: Site of anticonvulsant activity mediated by γ-aminobutyric acid. Science (80-) 1982. https://doi.org/10.1126/science.7146907.
[13] Velíšek L, Shang E, Velíšková J, Chachua T, Macchiarulo S, Maglakelidze G, et al. GABAergic neuron deficit as an idiopathic generalized epilepsy mechanism: The role of BRD2 haploinsufficiency in juvenile myoclonic epilepsy. PLoS One 2011. https://doi.org/10.1371/journal.pone.0023656.
[14] Ciumas C, Wahlin TBR, Jucaite A, Lindstrom P, Halldin C, Savic I. Reduced dopamine transporter binding in patients with juvenile myoclonic epilepsy. Neurology 2008. https://doi.org/10.1212/01.wnl.0000316120.70504.d5.
[15] Hu B, Wang D, Xia Z, Yang A, Zhang J, Shi Q, et al. Regulation and control roles of the basal ganglia in the development of absence epileptiform activities. Cogn Neurodyn 2020. https://doi.org/10.1007/s11571-019-09559-4.
[16] Gioanni Y, Gioanni H, Mitrovic N. Seizures can be triggered by stimulating non-cortical structures in the quaking mutant mouse. Epilepsy Res 1991. https://doi.org/10.1016/0920-1211(91)90043-F.
[17] Fernández-Guardiola A, Contreras CM, Calvo JM, Ayala F, Brailowsky S, Solis H, et al. Changes in Spontaneous Neuronal Firing in Cerebellum Red Nucleus and Raphe Nuclear Complex During Convulsive Activity. Cerebellum, Epilepsy, Behav 1974. https://doi.org/10.1007/978-1-4613-4508-4_2.
[18] Scheffer IE, Berkovic S, Capovilla G, Connolly MB, French J, Guilhoto L, et al. ILAE classification of the epilepsies: Position paper of the ILAE Commission for Classification and Terminology. Epilepsia 2017. https://doi.org/10.1111/epi.13709.

[19] Kwan P, Arzimanoglou A, Berg AT, Brodie MJ, Allen Hauser W, Mathern G, et al. Definition of drug resistant epilepsy: Consensus proposal by the ad hoc Task Force of the ILAE Commission on Therapeutic Strategies. Epilepsia 2010;51 (6):1069–77. https://doi.org/10.1111/j.1528-1167.2009.02397.x.
[20] Manjón JV, Bertó A, Romero JE, Lanuza E, Vivo-Hernando R, Aparici-Robles F, et al. pBrain: A novel pipeline for Parkinson related brain structure segmentation. NeuroImage Clin 2020. https://doi.org/10.1016/j.nicl.2020.102184.
[21] Glasser MF, Van Essen DC. Mapping human cortical areas in vivo based on myelin content as revealed by T1- and T2-weighted MRI. J Neurosci 2011;31 (32):11597–616. https://doi.org/10.1523/JNEUROSCI.2180-11.2011.
[22] Fukunaga M, Li TQ, van Gelderen P, de Zwart JA, Shmueli K, Yao B, et al. Layer-specific variation of iron content in cerebral cortex as a source of MRI contrast. PNAS 2010. https://doi.org/10.1073/pnas.0911177107.
[23] Basile GA, Quartu M, Bertino S, Serra MP, Boi M, Bramanti A, et al. Red nucleus structure and function: from anatomy to clinical neurosciences. Brain Struct Funct 2021. https://doi.org/10.1007/s00429-020-02171-x.
[24] Florio TM, Scarnati E, Rosa I, Di Censo D, Ranieri B, Cimini A, et al. The Basal Ganglia: More than just a switching device. CNS Neurosci Ther 2018. https://doi.org/10.1111/cns.12987.
[25] Bin G, Wang T, Zeng H, He X, Li F, Zhang J, et al. Patterns of gray matter abnormalities in idiopathic generalized epilepsy: A Meta-analysis of voxel-based morphology studies. PLoS One 2017. https://doi.org/10.1371/journal.pone.0169076.
[26] Hsin YL, Harnod T, Chang CS, Peng SJ. Increase in gray matter volume and white matter fractional anisotropy in the motor pathways of patients with secondarily generalized neocortical seizures. Epilepsy Res 2017. https://doi.org/10.1016/j.eplepsyres.2017.09.011.
[27] Meencke HJ, Janz D. The Significance of Microdysgenesia in Primary Generalized Epilepsy: An Answer to the Considerations of Lyon and Gastaut. Epilepsia 1985. https://doi.org/10.1111/j.1528-1157.1985.tb05665.x.
[28] Camlidag I, Kocabicak E, Sahin B, Jahanshahi A, Incesu L, Aygun D, et al. Volumetric analysis of the subthalamic and red nuclei based on magnetic resonance imaging in patients with Parkinson's disease. Int J Neurosci 2014. https://doi.org/10.3109/00207454.2013.843091.
[29] Chen S, Chen Y, Zhang Y, Kuang X, Liu Y, Guo M, et al. Iron Metabolism and Ferroptosis in Epilepsy. Front Neurosci 2020. https://doi.org/10.3389/fnins.2020.601193.
[30] Zimmer TS, David B, Broekaart DWM, Schidlowski M, Ruffolo G, Korotkov A, et al. Seizure-mediated iron accumulation and dysregulated iron metabolism after status epilepticus and in temporal lobe epilepsy. Acta Neuropathol 2021. https://doi.org/10.1007/s00401-021-02348-6.
[31] Whelan CD, Altmann A, Botía JA, Jahanshad N, Hibar DP, Absil J, et al. Structural brain abnormalities in the common epilepsies assessed in a worldwide ENIGMA study. Brain 2018. https://doi.org/10.1093/brain/awx341.
[32] Zhou SY, Tong L, Song F, Hong XJ, Sun HF, Chang H, et al. Selective medial temporal volume reduction in the hippocampus of patients with idiopathic generalized tonic-clonic seizures. Epilepsy Res 2015. https://doi.org/10.1016/j.eplepsyres.2014.11.014.
[33] Liu G, Lyu G, Yang N, Chen B, Yang J, Hu Y, et al. Abnormalities of diffusional kurtosis imaging and regional homogeneity in idiopathic generalized epilepsy with generalized tonic-clonic seizures. Exp Ther Med 2018. https://doi.org/10.3892/etm.2018.7018.
[34] Ferrie CD. Idiopathic generalized epilepsies imitating focal epilepsies. Epilepsia 2005. https://doi.org/10.1111/j.1528-1167.2005.00319.x.
[35] Walser G, Unterberger I, Dobesberger J, Embacher N, Falkenstetter T, Larch J, et al. Asymmetric seizure termination in primary and secondary generalized tonic-clonic seizures. Epilepsia 2009. https://doi.org/10.1111/j.1528-1167.2009.02068.x.
[36] Meeren H, Van Luijtelaar G, Lopes Da Silva F, Coenen A. Evolving concepts on the pathophysiology of absence seizures: The cortical focus theory. Arch Neurol 2005. https://doi.org/10.1001/archneur.62.3.371.
[37] Meeren HKM, Pijn JPM, Van Luijtelaar ELJM, Coenen AML, Da Silva FHL. Cortical focus drives widespread corticothalamic networks during spontaneous absence seizures in rats. J Neurosci 2002. https://doi.org/10.1523/jneurosci.22-04-01480.2002.
[38] Bancaud J, Talairach J, Morel P, Bresson M, Bonis A, Geier S, et al. "Generalized" epileptic seizures elicited by electrical stimulation of the frontal lobe in man. Electroencephalogr Clin Neurophysiol 1974. https://doi.org/10.1016/0013-4694(74)90031-5.
[39] Ossenblok P, van Houdt P, Colon A, Stroink H, van Luijtelaar G. A network approach to investigate the bi-hemispheric synchrony in absence epilepsy. Clin Neurophysiol 2019. https://doi.org/10.1016/j.clinph.2019.05.034.
[40] Goldsberry G, Mitra D, MacDonald D, Patay Z. Accelerated myelination with motor system involvement in a neonate with immediate postnatal onset of seizures and hemimegalencephaly. Epilepsy Behav 2011. https://doi.org/10.1016/j.yebeh.2011.06.025.
[41] Deodato F, Sabatelli M, Ricci E, Mercuri E, Muntoni F, Sewry C, et al. Hypermyelinating neuropathy, mental retardation and epilepsy in a case of merosin deficiency. Neuromuscul Disord 2002. https://doi.org/10.1016/S0960-8966(01)00312-1.
[42] Drenthen GS, Fonseca Wald ELA, Backes WH, Debeij-Van Hall MHJA, Hendriksen JGM, Aldenkamp AP, et al. Lower myelin-water content of the frontal lobe in childhood absence epilepsy. Epilepsia 2019. https://doi.org/10.1111/epi.16280.
[43] Schorner A, Weissert R. Patients with epileptic seizures and multiple sclerosis in a multiple sclerosis center in Southern Germany between 2003–2015. Front Neurol 2019. https://doi.org/10.3389/fneur.2019.00613.
[44] Baker J, Libretto T, Henley W, Zeman A. A Longitudinal Study of Epileptic Seizures in Alzheimer's Disease. Front Neurol 2019. https://doi.org/10.3389/fneur.2019.01266.
[45] Zhou Z, Tong Q, Zhang L, Ding Q, Lu H, Jonkman LE, et al. Evaluation of the diffusion MRI white matter tract integrity model using myelin histology and Monte-Carlo simulations. Neuroimage 2020. https://doi.org/10.1016/j.neuroimage.2020.117313.
[46] Lazari A, Lipp I. Can MRI measure myelin? Systematic review, qualitative assessment, and meta-analysis of studies validating microstructural imaging with myelin histology. Neuroimage 2021. https://doi.org/10.1016/j.neuroimage.2021.117744.
[47] Timmler S, Simons M. Grey matter myelination. Glia 2019. https://doi.org/10.1002/glia.23614.
[48] Zhang Z, Liao W, Chen H, Mantini D, Ding JR, Xu Q, et al. Altered functional-structural coupling of large-scale brain networks in idiopathic generalized epilepsy. Brain 2011;134(10):2912–28. https://doi.org/10.1093/brain/awr223.
[49] Lee HJ, Park KM. Structural and functional connectivity in newly diagnosed juvenile myoclonic epilepsy. Acta Neurol Scand 2019. https://doi.org/10.1111/ane.13079.
[50] McKavanagh A, Kreilkamp BAK, Chen Y, Denby C, Bracewell M, Das K, et al. Altered Structural Brain Networks in Refractory and Nonrefractory Idiopathic Generalized Epilepsy. Brain Connect 2021. https://doi.org/10.1089/brain.2021.0035.
[51] Fruengel R, Bröhl T, Rings T, Lehnertz K. Reconfiguration of human evolving large-scale epileptic brain networks prior to seizures: an evaluation with node centralities. Sci Rep 2020. https://doi.org/10.1038/s41598-020-78899-7.
[52] Lambert C, Zrinzo L, Nagy Z, Lutti A, Hariz M, Foltynie T, et al. Confirmation of functional zones within the human subthalamic nucleus: Patterns of connectivity and sub-parcellation using diffusion weighted imaging. Neuroimage 2012. https://doi.org/10.1016/j.neuroimage.2011.11.082.
[53] Vanegas-Arroyave N, Lauro PM, Huang L, Hallett M, Horovitz SG, Zaghloul KA, et al. Tractography patterns of subthalamic nucleus deep brain stimulation. Brain 2016. https://doi.org/10.1093/brain/aww020.
[54] Focke NK, Diederich C, Helms G, Nitsche MA, Lerche H, Paulus W. Idiopathic-generalized epilepsy shows profound white matter diffusion-tensor imaging alterations. Hum Brain Mapp 2014. https://doi.org/10.1002/hbm.22405.
[55] Jun YH, Eom TH, Kim YH, Chung SY, Lee IG, Kim JM. Source localization of epileptiform discharges in childhood absence epilepsy using a distributed source model: a standardized, low-resolution, brain electromagnetic tomography (sLORETA) study. Neurol Sci 2019. https://doi.org/10.1007/s10072-019-03751-4.
[56] Li N, Li J, Chen Y, Chu C, Zhang X, Zhong R, et al. One-Year Analysis of Risk Factors Associated With Cognitive Impairment in Newly Diagnosed Epilepsy in Adults. Front Neurol 2020. https://doi.org/10.3389/fneur.2020.594164.
[57] Schmalbach B, Günther V, Raethjen J, Wailke S, Falk D, Deuschl G, et al. The subthalamic nucleus influences visuospatial attention in humans. J Cogn Neurosci 2014. https://doi.org/10.1162/jocn_a_00502.
[58] Nioche C, Cabanis EA, Habas C. Functional connectivity of the human red nucleus in the brain resting state at 3T. Am J Neuroradiol 2009. https://doi.org/10.3174/ajnr.A1375.
[59] Moeller F, Maneshi M, Pittau F, Gholipour T, Bellec P, Dubeau F, et al. Functional connectivity in patients with idiopathic generalized epilepsy. Epilepsia 2011. https://doi.org/10.1111/j.1528-1167.2010.02938.x.
[60] Kros L, Eelkman Rooda OHJ, Spanke JK, Alva P, van Dongen MN, Karapatis A, et al. Cerebellar output controls generalized spike-and-wave discharge occurrence. Ann Neurol 2015. https://doi.org/10.1002/ana.24399.
[61] Joo EY, Hong SB, Tae WS, Han SJ, Seo DW, Lee KH, et al. Effect of lamotrigine on cerebral blood flow in patients with idiopathic generalised epilepsy. Eur J Nucl Med Mol Imaging 2006. https://doi.org/10.1007/s00259-005-0029-7.
[62] Reutens DC, Berkovic SF. Idiopathic generalized epilepsy of adolescence: Are the syndromes clinically distinct? Neurology 1995. https://doi.org/10.1212/WNL.45.8.1469.
[63] Benuzzi F, Mirandola L, Pugnaghi M, Farinelli V, Tassinari CA, Capovilla G, et al. Increased cortical BOLD signal anticipates generalized spike and wave discharges in adolescents and adults with idiopathic generalized epilepsies. Epilepsia 2012. https://doi.org/10.1111/j.1528-1167.2011.03385.x.